J. Earth Syst. Sci. (2025)134 190
https://doi.org/10.1007/s12040-025-02649-4

Nowcasting of rain with Doppler weather radar – A comparative strategy for complex orography

Swastika Chakraborty[1], Sumon Kumar Mondal[1], Bipasha Paul Shukla[2] and Saurabh Das[3,*]

[1]*Narula Institute of Technology, Kolkata, West Bengal 700 109, India.*
[2]*Space Application Centre, ISRO, Ahmedabad, India.*
[3]*Department of Astronomy, Astrophysics and Space Engineering, IIT Indore, Indore, Madhya Pradesh 453 552, India.*
**Corresponding author. e-mail: das.saurabh01@gmail.com saurabh.das@iiti.ac.in*

MS received 10 June 2024; revised 8 May 2025; accepted 14 June 2025

Nowcasting of North Eastern Himalayan orographic rainfall has been attempted using ground-based Doppler weather radar reflectivity echo information for more than 532 samples covering various rain events of the year 2023 over two densely populated hilly Indian locations, Agartala and Mohanbari. Various optical motion fields of rain are used as input to the nowcasting algorithm. Both ensemble and non-ensemble-based nowcasting algorithms have been used, and performances have been considered. Lead time of nowcast has been increased from half an hour to two hours. The performance analysis shows that there are significant seasonal and locational variations with respect to the statistical error parameter and contingency error parameter. With an increase in lead time, performance skill decreases. Use of a short-term ensemble prediction system in nowcasting with ensemble size varying from 24 to 72 does not indicate any significant improvement in performance. Detailed performance analysis of the algorithms will help in the efficient, targeted use of a suitable rain nowcasting algorithm for operational purposes.

Keywords. Nowcasting; orographic rain; Doppler weather radar; fractional skill score.

1. Introduction

Nowcasting of convective orographic initiation is a serious concern to be addressed with priority, as human habitat is increasing very fast in the foothills of the Himalayan region. The populated Indian hill region has a serious threat from landslides, cloud bursts, and flash floods due to the sudden change of microclimate dynamics. Sparse availability of ground rainfall information is the major challenge in the prediction of such sudden, devastating phenomena. Rainfall at hilly locations is very complex. It is found to increase with the increase in altitude and elevation up to a certain elevation, and beyond that, rainfall decreases (Shrestha *et al.* 2012). The shape of the hills and topographical geometry causes orographic rainfall local enhancement (Smith 1979; Anders *et al.* 2006). Some studies present the leeward and windward variability of orographic precipitation and its spatial correlation at the outer and middle Himalayan region (Singh and Kumar 1997). For north eastern India (NEI), according to a recent report, there is a decrease in the seasonal trend of

Published online: 09 September 2025

mean rainfall over the recent years (Saha *et al.* 2023), however, the frequency and intensity of occurrence of extreme rainfall increased at a significant rate. The comparison of the rate of increase over the past decades indicates that the recent rate of increase is faster, even compared to the prediction given by Clausius-Clapeyron scaling (Zahan *et al.* 2021). However, an increasing trend cannot be observed with confidence, looking at the event count of 24 rain gauges from the tea gardens of NEI and the Indian Meteorological Department (IMD) datasets. Even variability is insignificant against the Gaussian white noise null hypothesis due to regional scale thermodynamical variation and circulation leading to convective inhibition. The increasing trend of mean convective available potential energy (CAPE) with a decreasing trend of moisture and convective inhibition energy (CINE) may be the potential reason for the lack of confidence in observations. Therefore, inclusion of not so severe but extreme event may increase the confidence level. CAPE (Chakraborty *et al.* 2015) triggers convection, increasing cloud liquid water content (Chen *et al.* 2020) and dissipation in the form of rain at a later stage of the convection life cycle.

Forecasting precipitation with a very short lead time following complex movement and growth of rain orography has been attempted using the extrapolation of the echo motion vector of radar observation over Switzerland. Successful validation of the result indicates the potential of Doppler weather radar (DWR) for such a purpose (Schmid *et al.* 1992). Real-time validation of the operation of the motion field using the Dynamic and Adaptive Radar Tracking of Storms (DARTS) algorithm has been proven to be useful for an extreme weather event in Collaborative and Adaptive Sensing of the Atmosphere (CASA) Integrative Project 1 experiment (Ruzanski *et al.* 2009). Very recently, the Lucas–Kanade (LK) method (Zhu and Dai 2022) has been used for optical motion field determination of tropical cyclone rainfall nowcasting. The Otaki Precipitation Estimation by Radar (OPERA) program of New Zealand uses radar rainfall estimation along with rain gauge and satellite observation for characterization of orographic enhancement of rain. The study found that most of the orographic enhancement is triggered by the convection process (Gray and Seed 2006) and the seeder/feeder process for a short period of time. The short-duration process results in a sudden, abrupt enhancement of rain rate. This shows the necessity of high-resolution ground-based radar observation as input for orographic rain forecasting purposes for a better understanding of convection. Despite numerous sources of noise from clutter, hardware electronics issues, attenuation, beam broadening, overshooting, yet meteorologists prefer radar to observe the precipitation and thunderstorm growth as high-precision observation (Germann and Joss 2004). Forecasting with a short lead time is really challenging using a Numerical Weather Prediction (NWP) model, as it takes time to initiate with the available data. A stochastic probabilistic precipitation forecasting scheme combines a high-resolution NWP model with extrapolated radar forecasts to achieve higher performance quality for the forecast of low-intensity stratiform rainfall (Liguori *et al.* 2012; Bowler *et al.* 2020). Short-Term Ensemble Prediction System (STEPS) is an improved version of spectral prognosis (SPROG) (Reinoso-Rondinel *et al.* 2022), which analyzes scale-dependent position changes of convective rain. Thus, a quantitative nowcasting field ensemble is created. Autoregressive nowcasting with vertical integrated liquid (ANVIL) has been successfully used to account for the spatial variability and scale dependence of predictability of growth and decay of vertical integrated liquid (VIL) (Pulkkinen *et al.* 2020) in a spatial scale of 1–11 km. This method is an improvement of the basic extrapolation method of short-term prediction, where a separate autoregressive integrated model is applied for each scale in Lagrangian coordinates. Cascade levels are assumed to be developed independently for forecasting purposes. All the discussed algorithms except extrapolation typically use semi-Lagrangian advection trajectories to find the motion field.

Nonetheless, NEI is one of the predicted vulnerable spots for mesoscale hydrological disasters in the upcoming years (Paul and Maity 2023), and, therefore, it is urgently needed to have an appropriate prediction model considering local thermodynamical sudden change leading to extreme events. With technological advancement, satellite observation, radar observation along with *in-situ* measurement are made available over a limited region (Banerjee *et al.* 2020). Thus, high resolution, near real time spatiotemporal observation of ground truth is of utmost necessity to estimate and forecast orographic rainfall.

Short-range Warning of Intense Rainstorms in Localized Systems-2 (SWIRLS-2) algorithm, a combination of Tracking of Radar Echoes by

Correlation (TREC) and Group tracking of radar echoes (GTrack) for tracking the storm movement of a storm followed by Multi-scale Optical flow by Variational Analysis (MOVA), has been used for prediction with a lead time of six hours using DWR input (Srivastava *et al.* 2012). It has been validated over Indian locations, Kolkata, Delhi and the neighbourhood area. MOVA is observed to better perform over TREC and GTrack in tracking small scale features of thunderstorm events. Warning Decision Support System (WDSS-II) has been used for nowcasting purpose with S-band DWR input information and a lead time of two hours over Indian location, Delhi for various monsoonal conditions such as deep convection of pre-monsoon (April–June) and post-monsoon (October–November), early pre-monsoon, winter convective lines and monsoonal wide convective echoes (Sen Roy *et al.* 2014). For the case of pre-monsoon, comparatively higher error in prediction of location and intensity has been observed due to not having much horizontal growth area, however, for the monsoon case, prediction error is less. The Advanced Regional Prediction System, another efficient tool for nowcasting purposes, has been used for three-hourly predictions over fifty-five Indian stations. It shows a better probability of detection (POD) and false alarm ratio (FAR) in the pre-monsoon period than in the monsoon period using DWR input information. However, depending on the frequency of the event, skill score is observed to vary from one region to another (Ray *et al.* 2015). Forecast and tracking the evolution of cloud clusters, a nowcast algorithm has been validated over the Indian region using the information from INSAT-3D Infrared Channel (10.8 μm), which is based on the prediction of Mesoscale Convective Systems by Cloud Top Brightness Temperature (CTBT) extrapolation. Direct position error (DPE) in terms of the location of minimum CTBT is observed to vary from 70 to 144 km for a lead time of 30–180 min, respectively (Goyal *et al.* 2017). The prediction of rainfall caused by the North East Monsoon (NEM) over the south-eastern Indian peninsular region has been done using PySTEPS based nowcast model with the input from DWR (Raj *et al.* 2024). Reasonably good skill score has been found for a lead time of 120 min for a widespread rain persisting for a longer duration. Nowcasting of Extreme orographic Rain occurrences (NETRA) algorithm has been developed using INSAT-3D/3DR Hydro-Estimator (H-E) product for the western Himalayan region. It provides an alert for all over India for half an hour lead time with satisfactory performance (Singh *et al.* 2023). Optical flow-based algorithm, H-E Nowcaster, using the python-based library 'pysteps' (https://pysteps.github.io/) under creative common license is developed by Space Applications Centre, Indian Space Research Organization, for the purpose of nowcasting. The algorithm is successful in predicting precipitation fields up to the next six hours with the H-E data of INSAT-3DR satellite (https://www.mosdac.gov.in/heavyrain/assets/documents/Description_HEM_NOWCAST.pdf). India Meteorological Department-High Resolution Rapid Refresh (IMD-HRRR) model uses DWR network input and NWP model used for very short-range forecast to nowcast purpose. It shows improved performance for a forecast length up to 12 hours while validating with Metar, Synop, Buoy, and GPS-derived precipitable water over India (Srivastava *et al.* 2024).

The availability of indigenous dual polarization ground-based polarimetric high resolution near real time DWR information is an opportunity for the northeastern (NE) Himalayan hilly location Agartala (23.88°N, 91.25°E) and Mohanbari (27.46°N, 95.01°E) to be used for the nowcasting purpose of orographic rainfall. Here in this study, for the first time, the strategies of nowcasting of rain are compared for half an hour to two hours ahead of rainfall, considering ensemble-based as well as non-ensemble-based forecasting techniques for heavy and moderate spells of orographic rain over the hilly NE Himalayan region. This study will be helpful in choosing a strategy to generate an early warning message at the appropriate time for disaster management purposes.

2. Study area and data

The study area here is hilly tropical locations Agartala (23.88°N, 91.25°E) and Mohanbari (27.46°N, 95.01°E), as shown in figure 1, is very near to the Bay of Bengal (BOB). Typically, Agartala is a valley surrounded by hilly terrain and largely covered by forest. Due to the presence of the nearby ocean, there is fairly high humidity during summer. According to the Met Office report, the average annual temperature (both minimum and maximum) throughout the year 2023 is slightly higher than the average of the previous decade. For the year 2023, the highest and

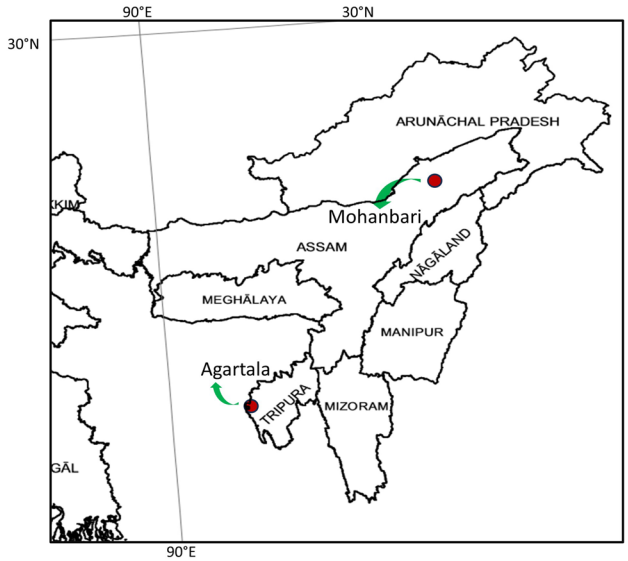

Figure 1. Study area.

lowest temperatures observed were 40.0° and 8.0°C, respectively. Due to southwesterly wind at the start of the month of June, monsoon sets in here and continue due to synoptic scale disturbances as occurred over the BOB in the east and the Arabian Sea in the west. Due to blockage by hills, heavy rain showers are frequent on the windward side, causing river overflow, flooding, landslides, etc., which continues up to the month of September every year. DWR scans of a 250 km area around Agartala and Mohanbari for the year 2023 are considered for the present nowcasting study of rain.

Initially, from raw radar input, Constant Altitude Plan Position Indicator (CAPPI) is developed using Python ARM Radar Toolkit, popularly known as PyART (Helmus and Collis 2016) to visualize, read, correct and analyze the data from weather radars. It is built on the Python ecosystem and can seamlessly integrate with radar libraries written in C to speed up computations. It is an open-source software that addresses the needs of the radar community. This makes it a useful tool for converting raw voltage measured by radar into spectra. Afterwards, the extraction of moments was done using signal processing. Correction and quality control are applied to flag and remove known artifacts. Rainfall amount, type, cloud and wind information are collected using retrieval algorithms.

Nowcasting for the next half an hour to two hours is then carried out with PySTEPS (Pulkkinen *et al.* 2019b), an open-source community-driven Python library for probabilistic rainfall nowcasting. The modular, well-documented and highly configurable structure of PySTEPS makes it suitable as a potential utility for warning system development in case of extreme weather prediction. A wide range of applications, such as the implementation of several optical flow methods and ensemble nowcasting using advanced stochastic generators, is supported by this library. Additionally, visualizing and postprocessing tools, deterministic nowcast tools and neighbourhood nowcast verification tools are available in this library to carry out scientific experiments and to understand the sensitivity of model parameters. Since the objective of this study is to explore the suitability of an algorithm for nowcasting of rainfall using high-resolution DWR reflectivity input from two different orographic locations, PySTEPS is well-suited for the purpose.

The range of the radar covers South Assam, Bangladesh, Tripura, Mizoram and the surrounding area. Medium range volume scan data for a maximum of nine minutes duration with ten minutes temporal interval are collected for the present study. A processed and filtered NetCDF file is considered in this study. Pulse repetition frequency of 1000 Hz is used here for this radar with an operating wavelength of 10 cm at S band, suitable to detect raindrops associated with intense rainfall. The scanning of radar is going on throughout the day with ten elevation angles up to 21°. The range of CAPPI used here is 250 km and at a height of 2.5 km. The height of the CAPPI is chosen to cover the entire operational range of the radar according to the elevation angle. DWR picks up echo information with a temporal resolution of ten minutes.

Rain rate is estimated from CAPPI reflectivity using well-known Marshal Palmer relation.

$$z = ar^b, \tag{1}$$

$a = 200$, $b = 1.6$ (Skolnik 1980).

Table 1 presents the statistics of three selected rainfall categories based on the gridded categorical verification methodology using the IMD gridded rainfall dataset (https://www.data.gov.in/catalog/rainfall) for this study.

Wind speed associated with 850 hPa for a typical sample of heavy rainfall category of the 5th July, 2023 is shown in figure 2(A). Wind speed associated with 850 hPa for a typical sample from the moderate rainfall category of 28th June, 2023 is shown in figure 2(B) over Agartala. Weak outgoing

longwave radiation (OLR) is shown in figure 2(C) corresponding to heavy rain. OLR corresponding to 28th June 2023, shown in figure 2(D), has a higher percentage for the moderate rain case as compared to heavy rain.

Heavy rainfall associated with a visible deep depression having strong gusts of wind in figure 2(A) over a large surface area has been found over Dharmanagar, Tripura. The monsoon trough lies along the foothills of the Himalayas during this event. Therefore, convective activity was triggered by a combination of isolated cells and multiple cells during a long interval. Heavy rainfall is observed in more than one station within the operational range of DWR and sometimes lasts for 2–3 consecutive days. Comparatively weak wind can be noticed from figure 2(B) to intrude into the lower atmospheric layer, causing moderate rain. A low-pressure area is formed from cyclonic movement, which is initiated from the southern part of Bangladesh and the area adjacent to the BOB. It gradually moved towards the northeastern side and then transformed into a deep depression at the Bangladesh coast. In the next couple of days, it is weakened into a depression over the neighbourhood of Agartala, causing moderate rain in some parts of Agartala.

Table 1. *Categorical statistics of chosen rainfall for this study.*

Daily total rainfall accumulation (mm)	Category name	Available event count
65–115	Heavy	48
25–65	Moderate	207
<25	Light	277

3. Methodology

Rainfall from each of the categories, such as heavy, moderate and light, is considered for optical motion field estimation and described in the subsequent section. The estimated motion field is considered as input of various nowcasting algorithms to understand the suitability of operational use of that particular algorithm for the case study, depending on location, microclimate, and availability of input. For nowcasting purpose, consecutive rainfall observation of 90 min is used for understanding the sequence of the next 120 min of prediction. Therefore, the next 120 min of observation is used as a validation dataset for each case. A sliding window variation of each 90 min observation for 12 time frames adds robustness to the performance evaluation of the model.

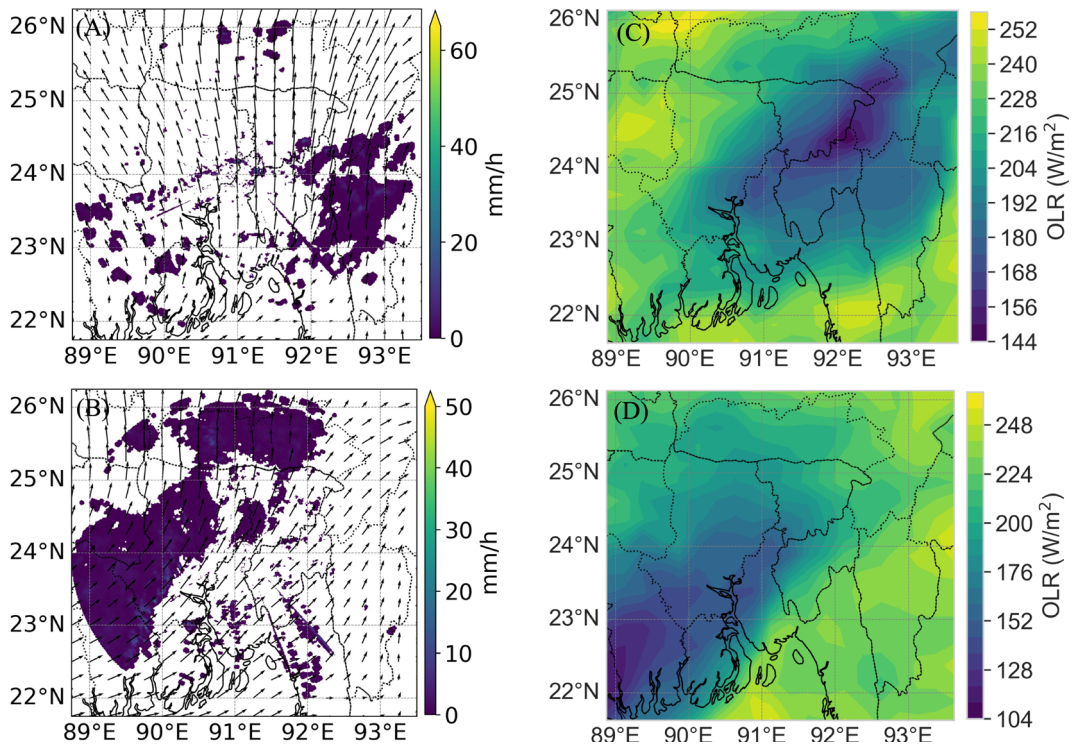

Figure 2. Synoptic condition of wind direction at 850 hPa over DWR reflectivity extracted rain rate of Agartala during (**A**) heavy rain and (**B**) moderate rain. Synoptic condition of OLR of Agartala during (**C**) heavy rain and (**D**) moderate rain.

Major challenge in the real-time rainfall forecasting is associated with the precise knowledge of micro-level change of instant of initiation, dissipation, decay, or growth at the spatiotemporal scale, which may not always be explained with the help of preset governing laws of thermodynamics. It is computationally very complicated to take care of all the associated thermodynamic processes, such as radiation, evaporation, condensation, and melting, to keep the spatiotemporal track of rainfall occurrence. The situation is more challenging for such a type of estimation when a hill, as an obstruction itself, is the source of uncertainty. Lagrangian persistence alone is not enough to visualize it properly. The sensible heat pattern of the cloud cluster (Robert 1982) is required to understand tropical large-scale vertical motion associated with stratiform as well as convective precipitation.

4. Optical motion

The spectral method (motion field) has been proven successful for nowcasting of rain based on radar data. Motion field using DARTS (Pulkkinen *et al.* 2019a) for heavy and moderate rain is shown in figure 3(A and B), respectively. Similarly, the motion field using the LK (Hambali *et al.* 2020; Ha and Lee 2024) method for heavy rain and moderate rain is shown in figure 3(C and D), respectively. All motion fields are used here to assess the applicability and efficacy of rain nowcasting of the NE Himalayan orographic region. Two categories are shown here only for simplicity of explanation. The discrete Fourier transform (DFT) is used in the DARTS method for smooth motion estimation by suitably truncating DFT coefficients while using a long time series of radar input. LK requires only two, sometimes more images, to track the local feature with a final interpolation step for smoothing. Basically, the motion field here is governed by the recursion equation at each cascade level.

$$R_j(x,y,t) = \sum_{k=1}^{2} \Phi_{j,k} R_j(x,y,t-k\Delta t) + \Phi_{j,0} \in_j (x,y,t), \quad (2)$$

where the first term indicates the deterministic part of Lagrangian persistence and the second term is a random perturbation. Random perturbation is generated with a Gaussian random field as residue after filtering with Fast Fourier Transform (FFT). Here, Δt is the difference between two consecutive rain fields, R_j is the time lagged auto correlation coefficient normalized to zero mean and unit variance, $\Phi_{j,k}$ is derived from $R_{j,k}$ for $k = 1, 2$ of Yule–Walker equations (Hamilton and Susmel 1994). Temporal variation at each level of the cascade undergoes a separate second-order autoregressive process to take care of dynamic scaling. Perturbation field is thereby unique for each ensemble member (Imhoff *et al.* 2020; Han *et al.* 2022). Therefore, for operational purposes, depending on the requirement and availability of input, the algorithm for motion field development can be opted.

5. Nowcasting algorithms

As previously mentioned, the quantitative estimation of nowcasting of rain at the synoptic scale with sufficient accuracy for a hilly region is very challenging due to the complexity of the spatial dynamics of rain cell formation and tracking. Moreover, the error in prediction comes from the conversion of reflectivity to rain rate for the case of radar measurement. Tracking of the feature of advection and its signature during the convection life cycle is analyzed in this work with different nowcasting algorithms. Towards this end, high-resolution data availability is a requirement to avoid loss of information; however, the accuracy of prediction is limited to a certain lead time only. Here for the operational nowcasting purpose over NE Himalayan hill region, the performance of deterministic algorithm, ANVIL and SPROG are compared with probabilistic algorithm STEPS with variable ensemble size. This analysis will provide potential insight into the applicability of nowcasting algorithms to develop an early warning system in case of severe rainfall situations over the NE Indian hill orographic region.

5.1 *Ensemble-based and non-ensemble-based nowcasting*

In ensemble-based nowcasting, STEPS plays a major role in injecting random chaotic conditions at the time of initiation of the model. It considers bandpass filtering and cascaded decomposition-based nowcasting. Ensemble forecasting (Bringi and Chandrasekar 2001; Doviak 2006) is especially useful for incorporating uncertainties in modelling to extract more information from available data.

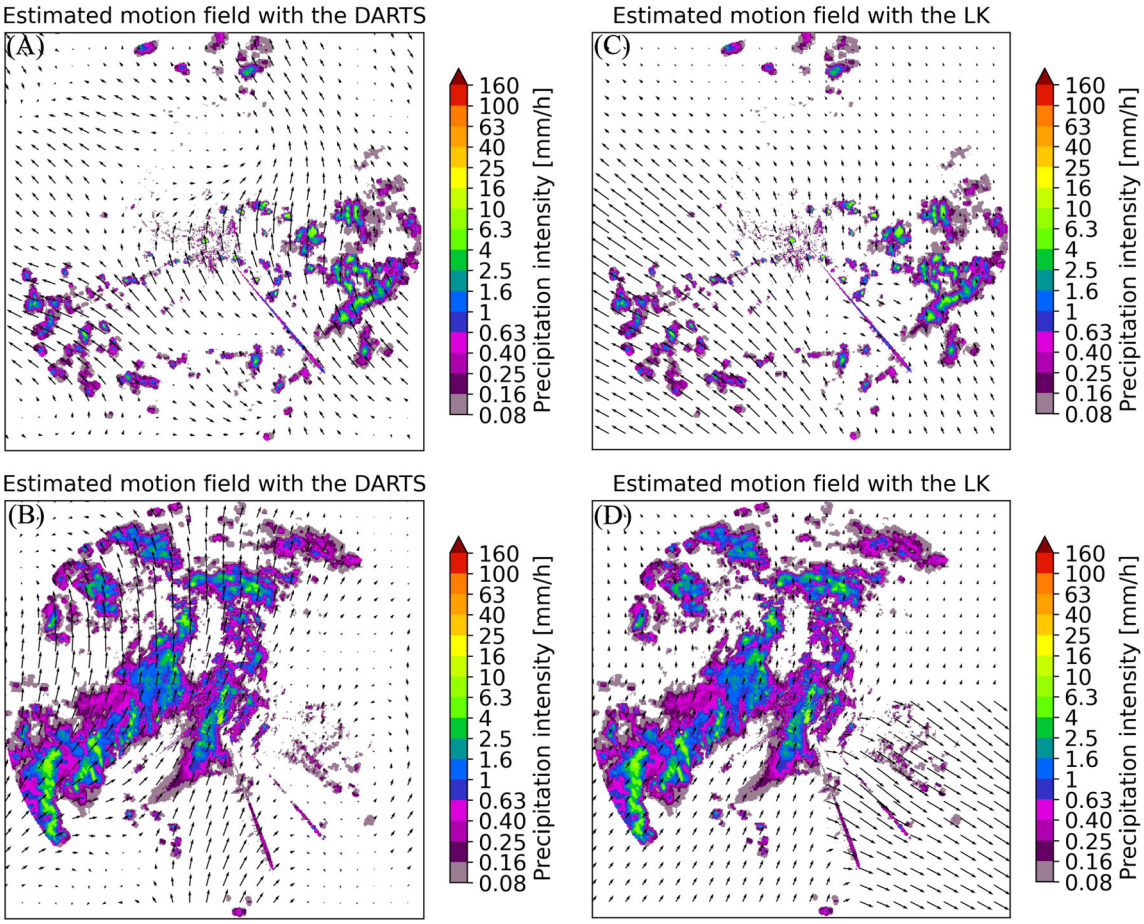

Figure 3. Optical flow using DARTS method of (**A**) heavy rain and (**B**) moderate rain. Optical flow using LK method of (**C**) heavy rain and (**D**) moderate rain.

This strategy of forecasting results in higher accuracy and better reliability and is very useful as a decision support tool. A heavy rain event of 5th July 2023 over Agartala is shown in figure 4(A). Nowcasting by the ensemble method of that heavy rain using STEPS with ensemble sizes 24, 48 and 72 with lead time of 30, 60, 90 and 120 min is shown in figure 4(B–D), respectively. The simplest algorithm for nowcasting purposes is non-ensemble-based advection-based extrapolation, where the semi-Lagrangian extrapolation method is used as input with two-dimensional array of one rain field instance. The time stamp is derived from the advection velocity to generate a three-dimensional rain field. DARTS is used for motion field generation here. ANVIL requires at least four instances of rain field for nowcasting, whereas simple extrapolation requires one. Here, the growth and decay pattern of rain is conceived in a more generalized way. A two-dimensional array from cascaded FFT decomposition of multiscale second-order autoregressive integration with the time derivative of the rain series is considered as input here. An empirical relation is used for rain rate series generation from VIL. Better spatial coverage is attempted with a moving window technique for estimation. Nowcasting of a typical heavy rain event of 5th July 2023 for Agartala with a lead time of 30, 60, 90 and 120 min is shown using extrapolation in figure 4(E), using ANVIL in figure 4(F) and using SPROG in figure 4(G).

A moderate rain event of 28th June 2023 over Agartala is shown in figure 5(A). Nowcasting by the ensemble method of that heavy rain using STEPS with ensemble sizes 24, 48 and 72 with lead time of 30, 60, 90 and 120 min is shown in figure 5(B–D), respectively. Nowcasting of the moderate rain event of 28th June 2023 for Agartala with a lead time of 30, 60, 90 and 120 min is shown using non-ensemble-based algorithm, such as extrapolation in figure 5(E), ANVIL in figure 5(F) and SPROG in figure 5(G).

A heavy rain event of 8th July 2023 over Mohanbari is shown in figure 6(A). Nowcasting by

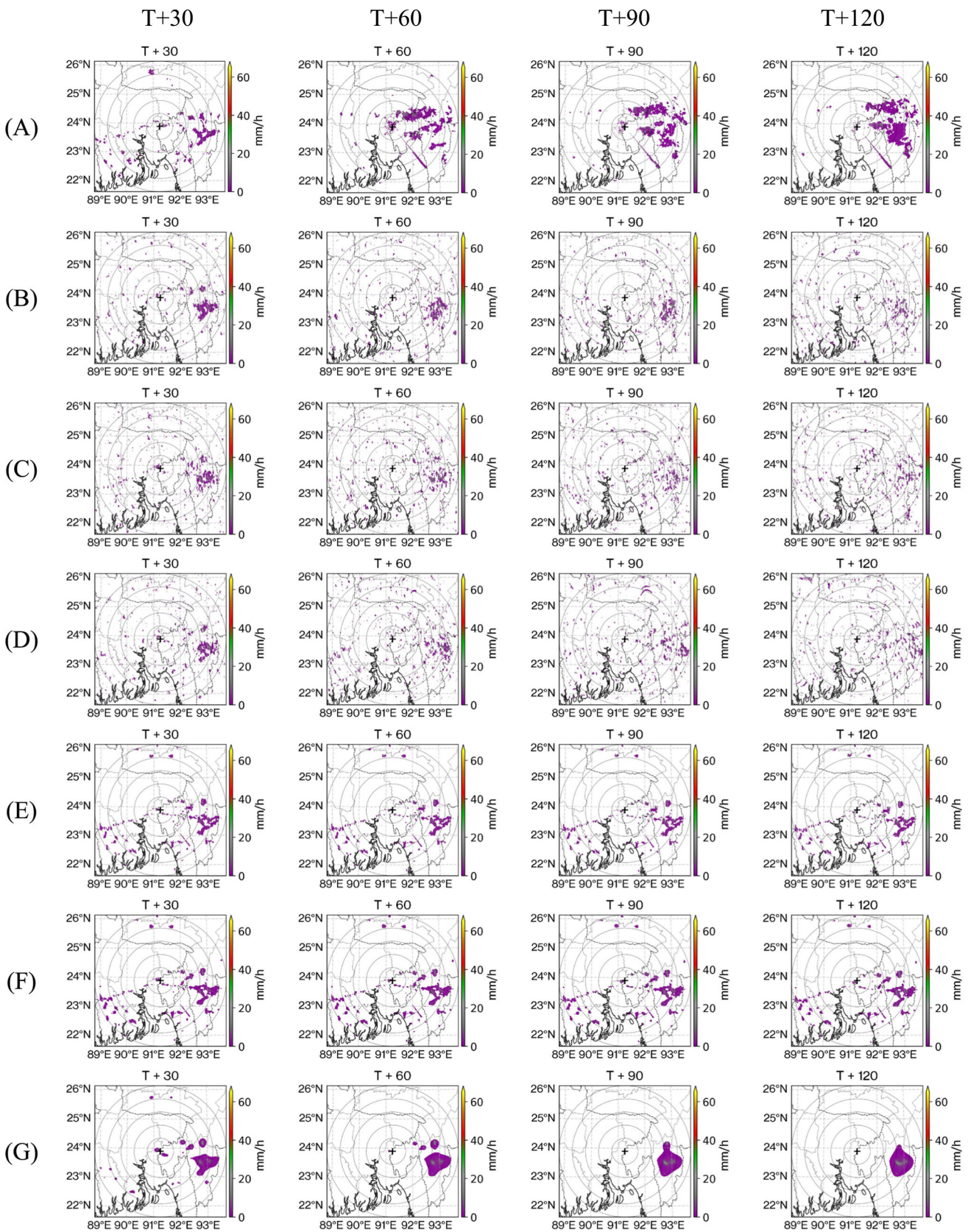

Figure 4. Heavy rain for Agartala (**A**) observed rainfall with lead time; nowcasted rainfall with lead time for ensemble size (**B**) 24, (**C**) 48 and (**D**) 72; nowcasted rainfall with lead time for (**E**) extrapolation, (**F**) ANVIL and (**G**) SPROG.

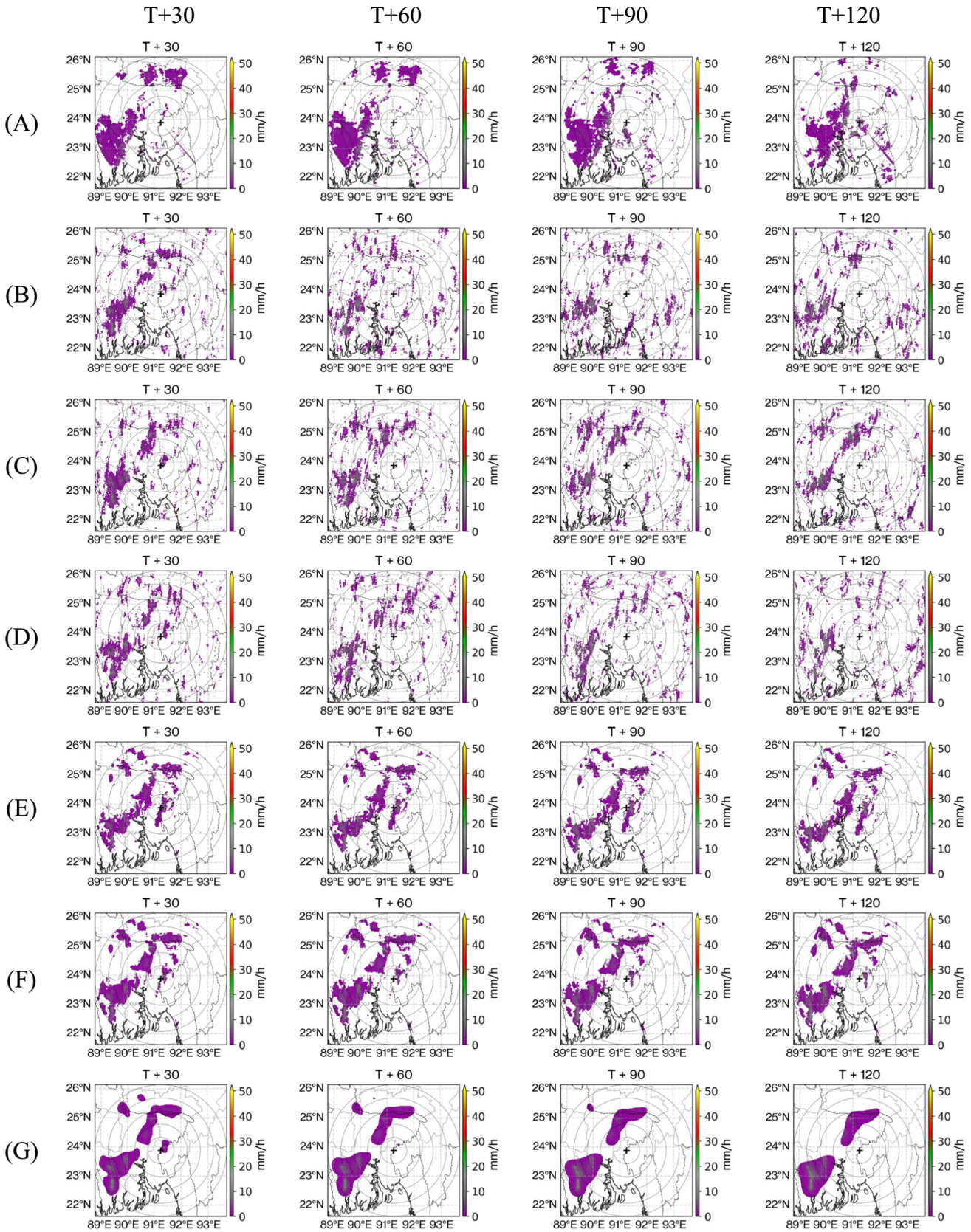

Figure 5. Moderate rainfall for Agartala (**A**) observed rainfall with lead time; nowcasted rainfall with lead time for ensemble size (**B**) 24, (**C**) 48 and (**D**) 72; nowcasted rainfall with lead time for (**E**) extrapolation, (**F**) ANVIL, and (**G**) SPROG.

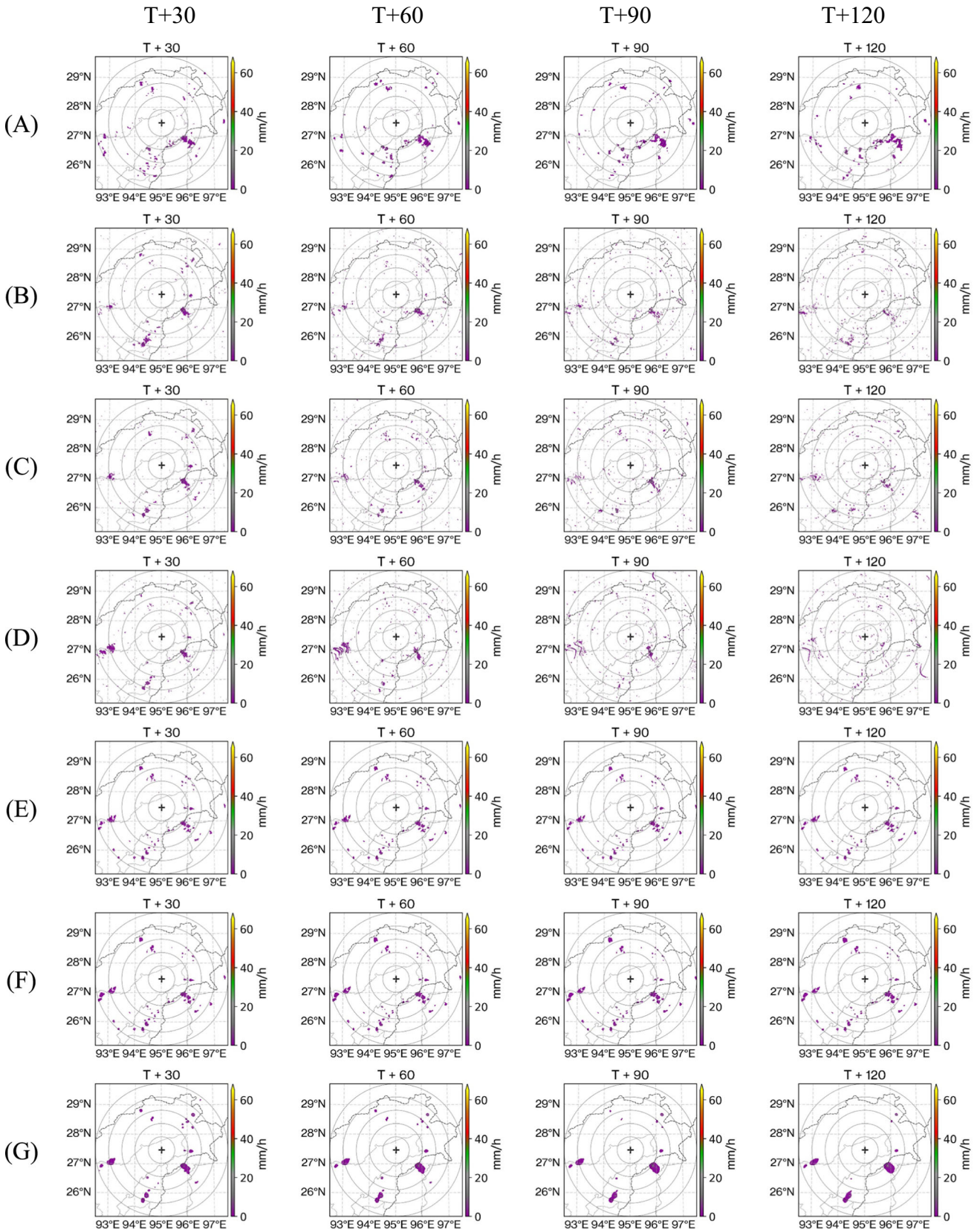

Figure 6. Heavy rainfall for Mohanbari (**A**) observed rainfall with lead time; nowcasted rainfall with lead time for ensemble size (**B**) 24, (**C**) 48 and (**D**) 72; nowcasted rainfall with lead time for (**E**) extrapolation, (**F**) ANVIL, and (**G**) SPROG.

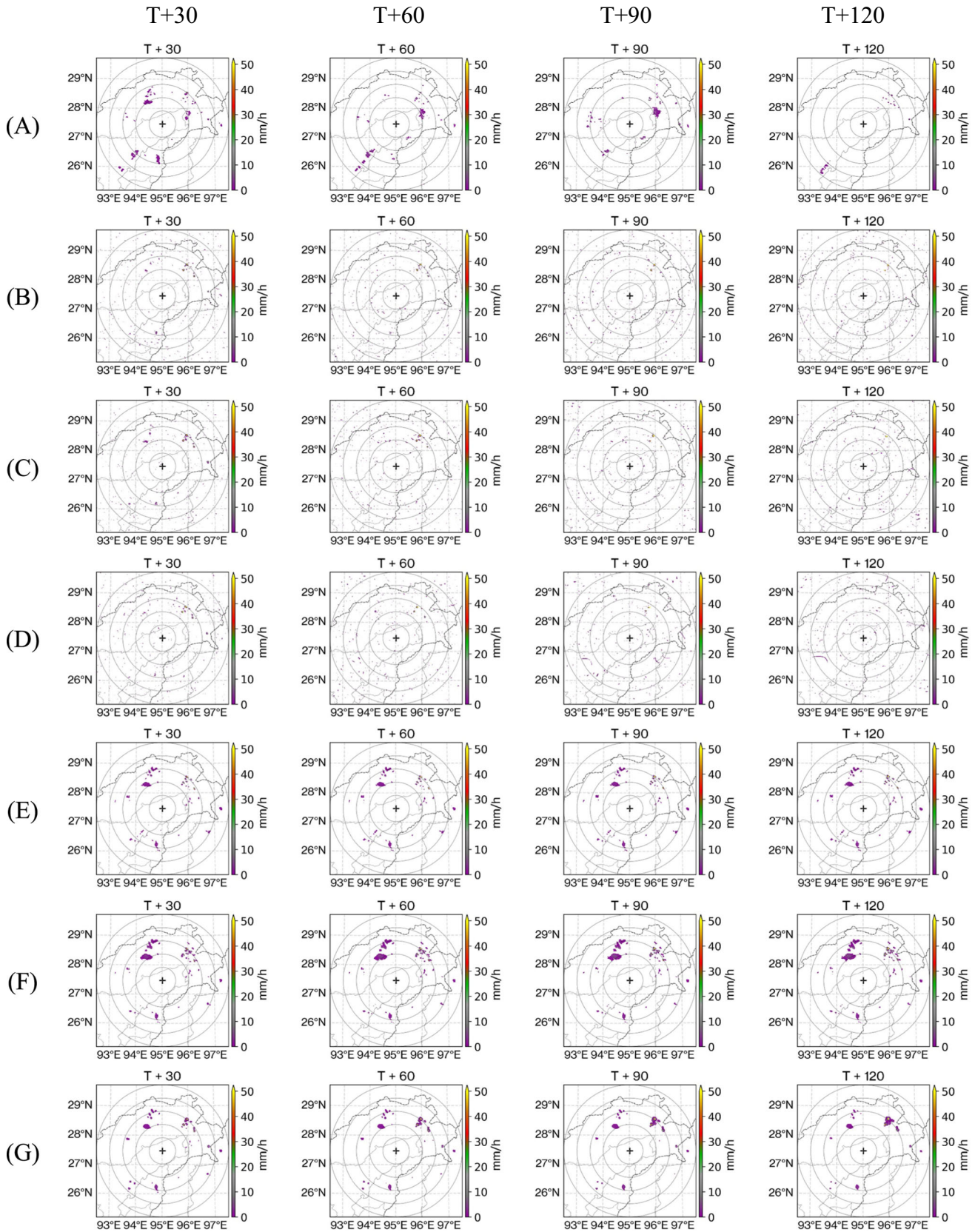

Figure 7. Moderate rainfall for Mohanbari (**A**) observed rainfall with lead time; nowcasted rainfall with lead time for ensemble size (**B**) 24, (**C**) 48 and (**D**) 72; nowcasted rainfall with lead time for (**E**) extrapolation, (**F**) ANVIL, and (**G**) SPROG.

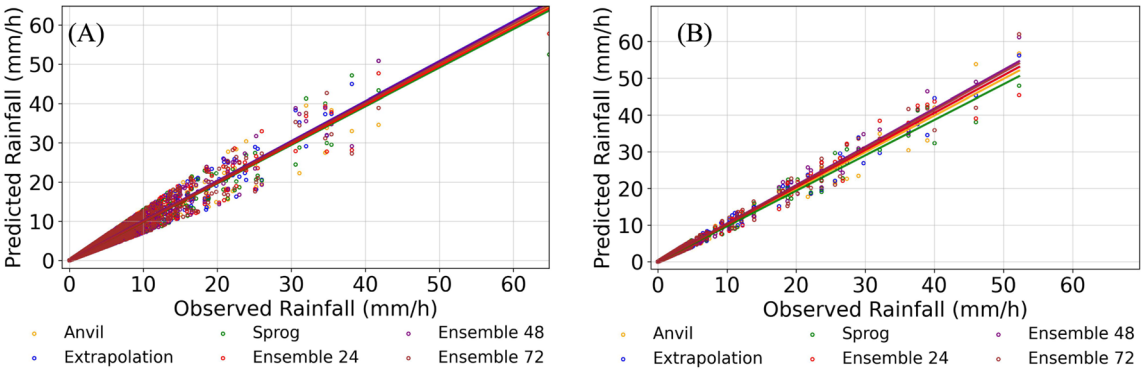

Figure 8. Scatter plot of observation *vs.* prediction for (**A**) heavy and (**B**) moderate rain.

ensemble method of that heavy rain using STEPS with ensemble sizes 24, 48 and 72 with lead time of 30, 60, 90 and 120 min is shown in figure 6(B–D), respectively. Nowcasting of a typical heavy rain event of 8th July 2023 for Mohanbari with a lead time of 30, 60, 90 and 120 min is shown using non-ensemble-based algorithm, such as extrapolation in figure 6(E), ANVIL in figure 6(F) and SPROG in figure 6(G).

A moderate rain event of 22nd June 2023 over Mohanbari is shown in figure 7(A). Nowcasting by the ensemble method of that heavy rain using STEPS with ensemble sizes 24, 48 and 72 with lead time of 30, 60, 90 and 120 min is shown in figure 7(B–D), respectively. Nowcasting of moderate rain event of 22nd June 2023 for Mohanbari with a lead time of 30, 60, 90 and 120 min is shown using non-ensemble-based algorithms, such as extrapolation in figure 7(E), ANVIL in figure 7(F) and SPROG in figure 7(G).

All the methods are executed with a cascade size of six. Looking at the spatial distribution of nowcasting algorithms, many spatial features in the observations are missing in the prediction, even for the 30 min ahead forecast. It may be due to the widespread of instances for ensemble-based prediction, as the nowcasting here produces ensemble of instances instead of a single instance. Nowcasting is better for all categories of rain with increasing ensemble size, however, for the case of ensemble size 72 and two hours of lead time the prediction is not so good. Of course, increasing ensemble size is very challenging considering computational hardware and the time of computation. As the backbone of STEPS is extrapolation, therefore to generate a new rain field, the algorithm is dependent on the past rain field. However, as per synoptic meteorology, the other dependencies of rainfall, such as wind, OLR, temperature, and humidity are also to be considered simultaneously at the time of nowcasting. This may be the potential reason for not getting the maximum similarity of the predicted image with the observed image.

Extrapolation is used as a traditional method of nowcasting based on Lagrangian, however, it cannot extract information at the time of growth and decay of convection. Reflectivity series is transformed into the spectral domain using FFT at the first step of S-PROG (Wilson *et al.* 1998, 2004). Over the cascaded decomposed series, a band-pass filter based on the Gaussian window is used for the appropriate frequency selection purpose. Afterwards, the calculation of the inverse transform was done to get back into the spatial domain. SPROG, when combined with the autoregressive (AR) method, leads to ANVIL. ANVIL processes information on the scale-dependent growth and decay of VIL by an autoregressive integration (ARI) process. Decomposition of VIL into variable spatial scale has been done here before integration is applied for each scale. In this way, it better replicates the actual observation. Location and intensity of prediction for both the cases of Agartala and Mohanbari are acceptable, however, the figure shows very little information with respect to location as per the availability of the rainfall event captured by DWR. It is observed that, irrespective of the category of event, with increasing lead time, nowcast quality is compromised. However, ANVIL and SPROG are found to capture the event comparatively better among all three algorithms used here.

6. Performance analysis

Figure 8(A and B) shows a scatter plot of predicted rainfall with observed rainfall of heavy and moderate rainfall days, respectively. Comparing the

performance of both types of rain, a slightly greater variability for heavy rain prediction is visible. The figure is plotted for the prediction with a lead time of 30 min. For the case of 60 and 90 min lead time, the inference from the prediction-observation scatter plot is the same. The inclusion of synoptic dependencies as input may reduce the deviation in the predicted result from the observation. DWR extracted rainfall observation corrected with dense gauge network observation will also improve the prediction performance. Overall seasonal performance shows that ANVIL is better as increased amount of data produces a better learning pattern for nowcasting. However, extrapolation may also be used for operational purposes based on the microclimatic influence of a particular day.

For operational nowcasting purposes, the appropriate use of an algorithm is required to apply in advance with sufficient time without hampering the quality of prediction. Statistical error parameters such as root mean square error (RMSE), mean absolute error (MAE) and Pearson correlation coefficient (PCC) are, hence, calculated.

Table 2. *Performance metrics of light category of rainfall across nowcasting algorithm.*

Name of algorithm	Performance parameter (maximum)	Agartala leadtime (min)				Mohanbari leadtime (min)			
		30	60	90	120	30	60	90	120
24	RMSE	0.25	0.27	0.51	0.37	1.03	1.00	1.05	1.08
	MAE	0.06	0.06	0.06	0.07	0.11	0.11	0.13	0.13
	FSS	0.94	0.88	0.84	0.69	0.92	0.84	0.78	0.72
	CSI	0.68	0.58	0.53	0.46	0.52	0.43	0.40	0.34
	POD	0.70	0.60	0.55	0.49	0.54	0.45	0.42	0.35
	FAR	0.06	0.08	0.08	0.28	0.05	0.09	0.12	0.17
48	RMSE	0.25	0.27	0.51	0.37	1.03	1.00	1.05	1.08
	MAE	0.06	0.06	0.06	0.07	0.11	0.11	0.13	0.13
	FSS	0.93	0.88	0.79	0.67	0.92	0.85	0.78	0.72
	CSI	0.68	0.58	0.53	0.46	0.52	0.43	0.40	0.34
	POD	0.70	0.60	0.55	0.49	0.54	0.45	0.42	0.35
	FAR	0.06	0.08	0.08	0.28	0.05	0.09	0.12	0.17
72	RMSE	0.25	0.27	0.51	0.37	1.03	1.00	1.05	1.08
	MAE	0.06	0.06	0.06	0.07	0.11	0.11	0.13	0.13
	FSS	0.94	0.88	0.84	0.69	0.92	0.85	0.78	0.72
	CSI	0.68	0.58	0.53	0.46	0.52	0.43	0.40	0.34
	POD	0.70	0.60	0.55	0.49	0.54	0.45	0.42	0.35
	FAR	0.06	0.08	0.08	0.28	0.05	0.09	0.12	0.17
ANVIL	RMSE	0.25	0.27	0.51	0.37	1.03	1.00	1.05	1.08
	MAE	0.06	0.06	0.06	0.07	0.11	0.11	0.13	0.13
	FSS	0.97	0.94	0.88	0.75	0.92	0.85	0.78	0.72
	CSI	0.68	0.58	0.53	0.46	0.52	0.43	0.40	0.34
	POD	0.70	0.60	0.55	0.49	0.54	0.45	0.42	0.35
	FAR	0.06	0.08	0.08	0.28	0.05	0.09	0.12	0.17
Extrapolation	RMSE	0.25	0.27	0.51	0.37	1.03	1.00	1.05	1.08
	MAE	0.06	0.06	0.06	0.07	0.11	0.11	0.13	0.13
	FSS	0.97	0.94	0.88	0.75	0.92	0.85	0.78	0.72
	CSI	0.68	0.58	0.53	0.46	0.52	0.43	0.40	0.34
	POD	0.70	0.60	0.55	0.49	0.54	0.45	0.42	0.35
	FAR	0.06	0.08	0.08	0.28	0.05	0.09	0.12	0.17
SPROG	RMSE	0.25	0.27	0.51	0.37	1.03	1.00	1.05	1.08
	MAE	0.06	0.06	0.06	0.07	0.11	0.11	0.13	0.13
	FSS	0.97	0.94	0.88	0.75	0.92	0.85	0.78	0.72
	CSI	0.68	0.58	0.53	0.46	0.52	0.43	0.40	0.34
	POD	0.70	0.60	0.55	0.49	0.54	0.45	0.42	0.35
	FAR	0.06	0.08	0.08	0.28	0.05	0.09	0.12	0.17

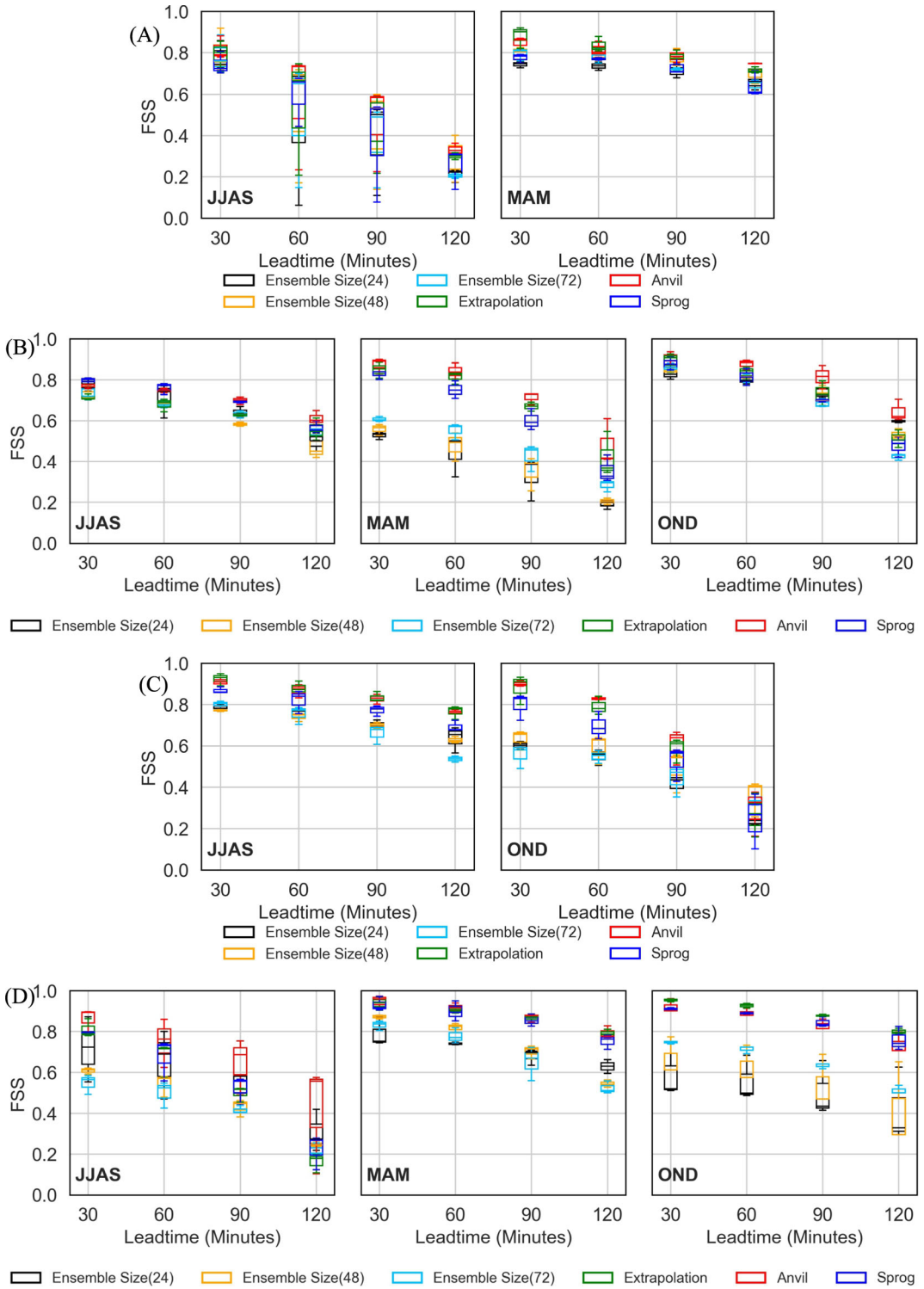

Figure 9. Seasonal performance of FSS (**A**) heavy and (**B**) moderate rain for Agartala; (**C**) heavy and (**D**) moderate rain for Mohanbari.

RMSE is calculated as

$$RMSE = \sqrt{\sum_{i=1}^{n} \frac{(y_i - \hat{y}_i)^2}{n}}, \qquad (3)$$

where y_i is the actual value for the ith observation, $\hat{y}_i$ is the predicted value for the ith observation, and n is the number of observations.

MAE is calculated as

$$MAE = \sqrt{\sum_{i=1}^{n} \frac{|y_i - \hat{y}_i|}{n}}, \quad (4)$$

where y_i is the actual value for the ith observation, $\hat{y}_i$ is the predicted value for the ith observation, and n is the number of observations.

PCC is calculated as

$$PCC = \frac{\sum(x_i - \overline{x})(y_i - \overline{y})}{\sum (x_i - \overline{x})^2 \sum (y_i - \overline{y})^2}, \quad (5)$$

where x_i is the value of the x variable in a sample, $\overline{x}$ is the mean of the values of the x variable, y_i is the value of the y variable in a sample, and $\overline{y}$ is the mean of the values of the y variable.

Contingency error parameters are also calculated as follows:

Fractions skill score (FSS) (Roberts and Lean 2008) is used here for neighbourhood verification of high-resolution precipitation forecasts against radar rainfall estimation and can be written as:

$$FSS = 1 - \frac{\frac{1}{N}\sum_{i=1}^{N}\left(p_f - p_0\right)^2}{\frac{1}{N}\sum_{i=1}^{N}{p_f}^2 + \frac{1}{N}\sum_{i=1}^{N}{p_0}^2}, \quad (6)$$

where N is the number of grid point for a sliding window of given size, p_f is the forecast fraction, and p_0 is the observed fraction of the same sliding window.

Critical success index (CSI) can be formulated as

$$CSI = \frac{hits}{hits + misses + false\ alarm}. \quad (7)$$

POD can be formulated as

$$POD = \frac{hits}{hits + misses}. \quad (8)$$

FAR can be formulated as

$$FAR = \frac{false\ alarm}{hits + false\ alarm}. \quad (9)$$

Conventionally, FSS (Raj *et al.* 2024) is used unconditionally as the score parameter, which depends on the gridded pixel based on a figure of merit defined by the fraction of the pixel exceeding a predefined threshold from the neighbourhood. Therefore, initially, FSS is calculated to assess the nowcasting skill of all of our used models for the nowcasting of NE Indian hill locations. However, the threshold and the bias for FSS calculations are the two important sensitive parameters that may produce a misleading (Antonio and Aitchison 2023) decision. There is a displacement at the instant when the nowcast gives the shape of the object and when the actual object is there, which is parameterized through FSS. Displacement exceeding the threshold of FSS is correlated with the average displacement. Bias is also another important parameter to quantify the information gap between observation and forecast. CSI and POD are also calculated in addition to FSS here. FAR is studied with POD for each category of rainfall prediction to have an idea about the operational nowcasting model suitable for NE Indian Himalayan hilly region. The rainfall threshold is considered here to be 5 mm/hr for all the score calculations. Performance of heavy and moderate rain with respect to the error parameter is shown in the subsequent section, and typical findings of light rain are presented in table 2.

6.1 *Comparison of FSS*

The box-and-whisker plot of FSS is shown in figure 9(A and B) for heavy rain of 5th July 2023 and moderate rain of 28th June 2023 in Agartala, respectively. Figure 9(C and D) shows the same for heavy rain of 8th July 2023 and moderate rain of 22nd June 2023 in Mohanbari, respectively, as per the availability of the seasonal data. For heavy rain, FSS of pre-monsoon (March–April–May (MAM)) is found to be acceptable up to two hours of lead time for Agartala. It is, however, found to be very good for monsoon (June–July–August–September (JJAS)) for Mohanbari up to two hours of lead time, irrespective of the ensemble or non-ensemble-based nowcasting algorithm used. However, FSS during JJAS for Agartala and FSS during post-monsoon (October–November–December (OND)) for Mohanbari decrease rapidly as the lead time of forecast increases.

In comparison to all other non-ensemble-based methods, ANVIL performs comparatively better than other models, even with increasing lead time, irrespective of the location. This may be due to better spatial coverage of estimation by the moving window technique. Interestingly, FSS for the moderate category of rainfall is good up to two hours of lead time for Mohanbari during pre-monsoon, but for monsoon and post-monsoon, the performance decreases with the increase of lead time. For Agartala, monsoon and post-monsoon performances are very good till one and a half hours and performance degrades beyond the lead time of one and a half hours. The number of outliers across the dataset is very low, as observed from the figure, irrespective of season, however, depending on location and seasonal variation,

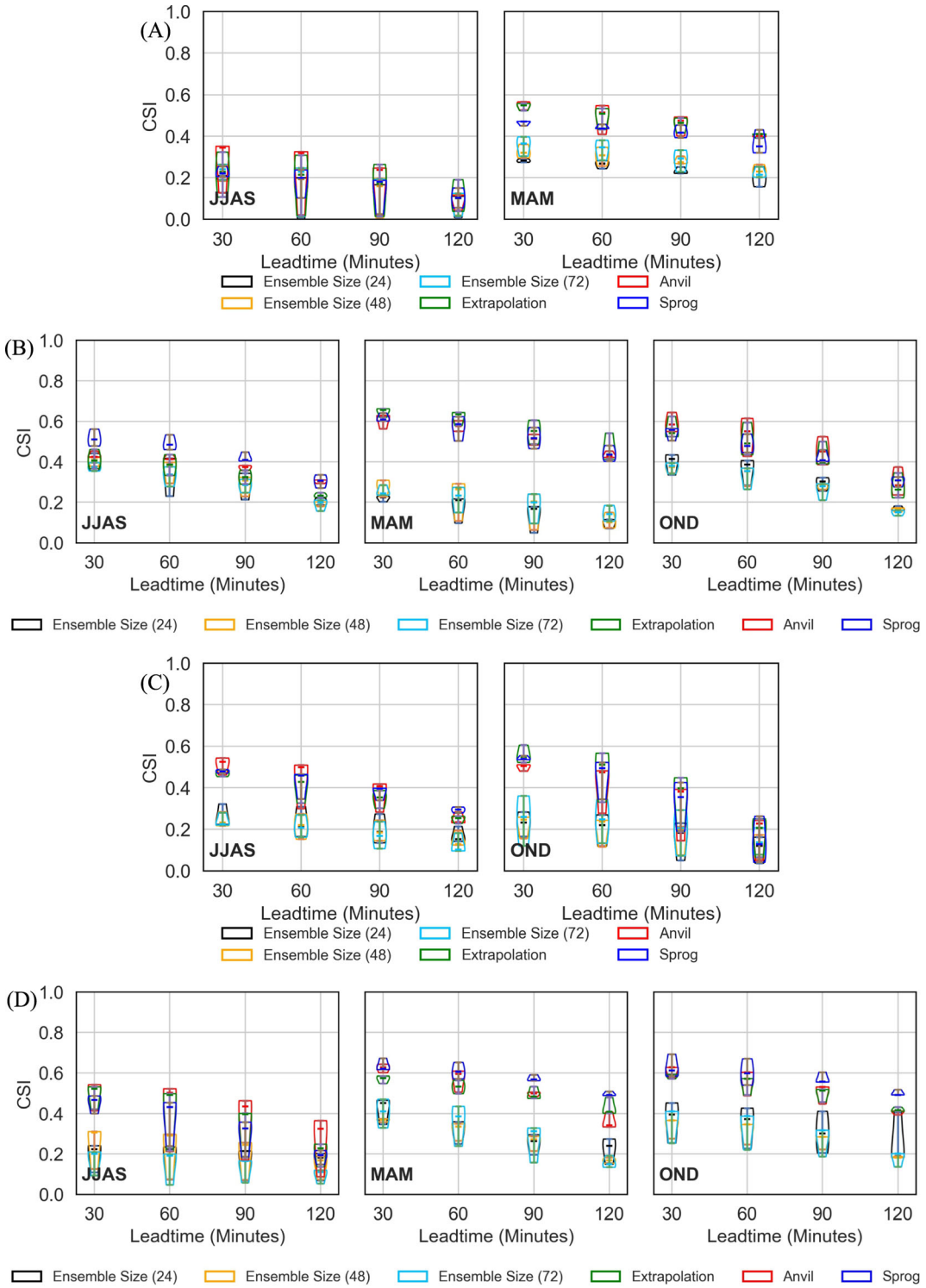

Figure 10. Seasonal performance of CSI (**A**) heavy and (**B**) moderate rain for Agartala; (**C**) heavy and (**D**) moderate rain for Mohanbari.

skewness is observed across the datasets. This may be due to the presence of some isolated convective activity giving misleading information after a certain lead time, mostly an hour.

Overall statistics indicate that both ANVIL and SPROG are acceptable options for the prediction of growth and decay, but there will be some information loss for small-scale features requiring an additional step of post-processing to correct the bias as a result of the autoregressive process. For the ANVIL method of nowcast, this post-processing is not required as small-scale features are already preserved.

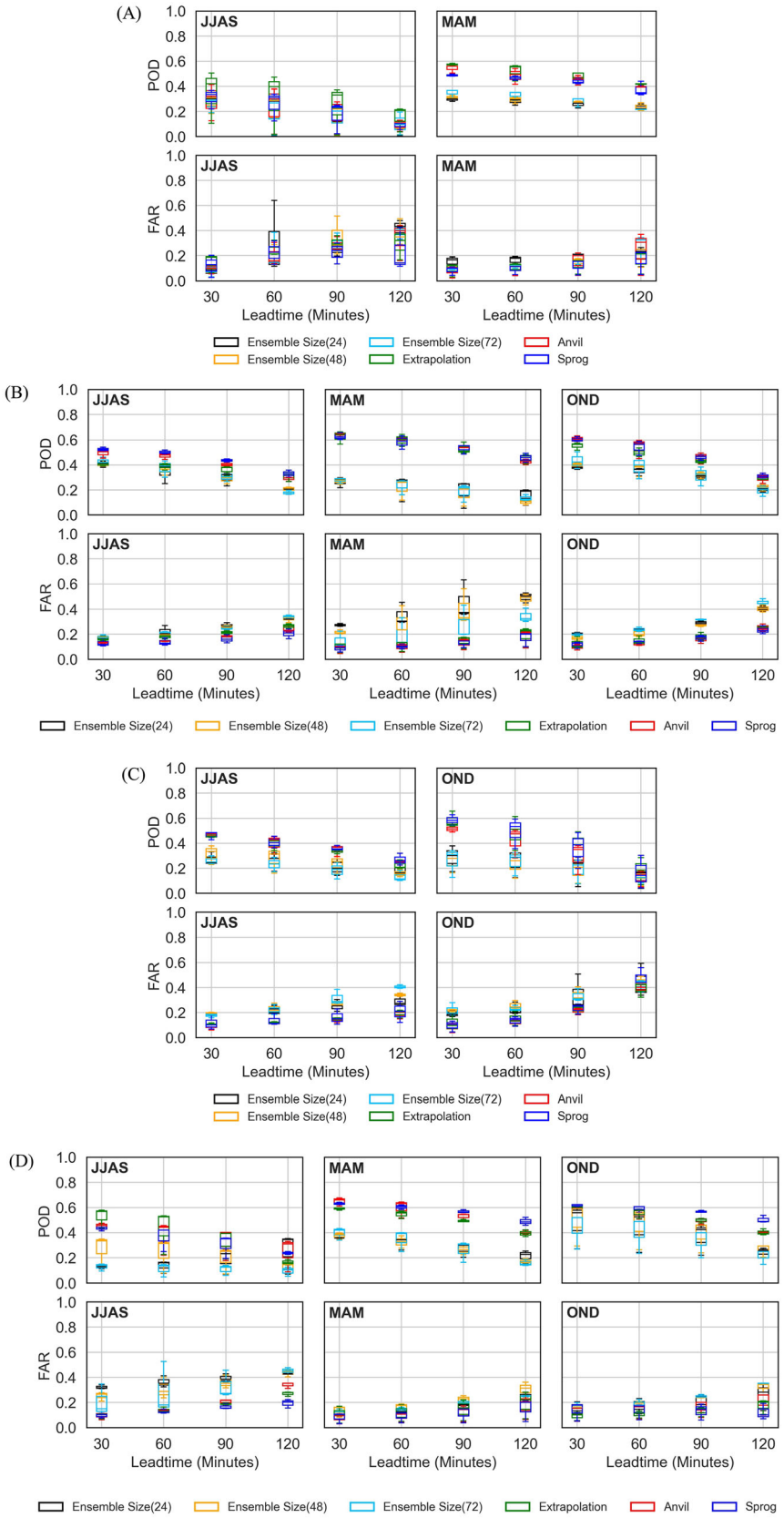

Figure 11. Seasonal performance of POD and FAR (**A**) heavy and (**B**) moderate rain for Agartala; (**C**) heavy and (**D**) moderate rain for Mohanbari.

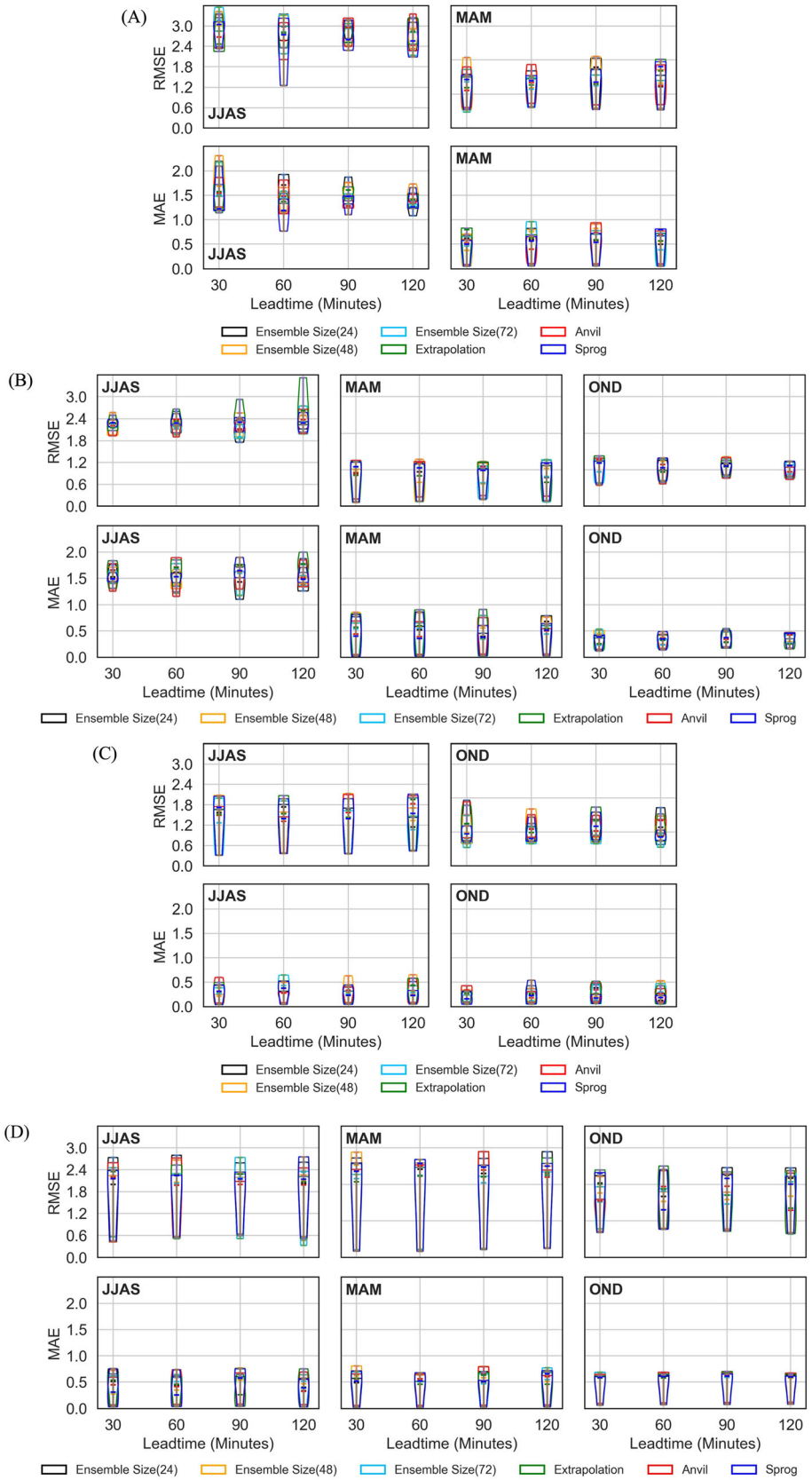

Figure 12. Seasonal performance of RMSE and MAE (**A**) heavy and (**B**) moderate rain for Agartala; (**C**) heavy and (**D**) moderate rain for Mohanbari.

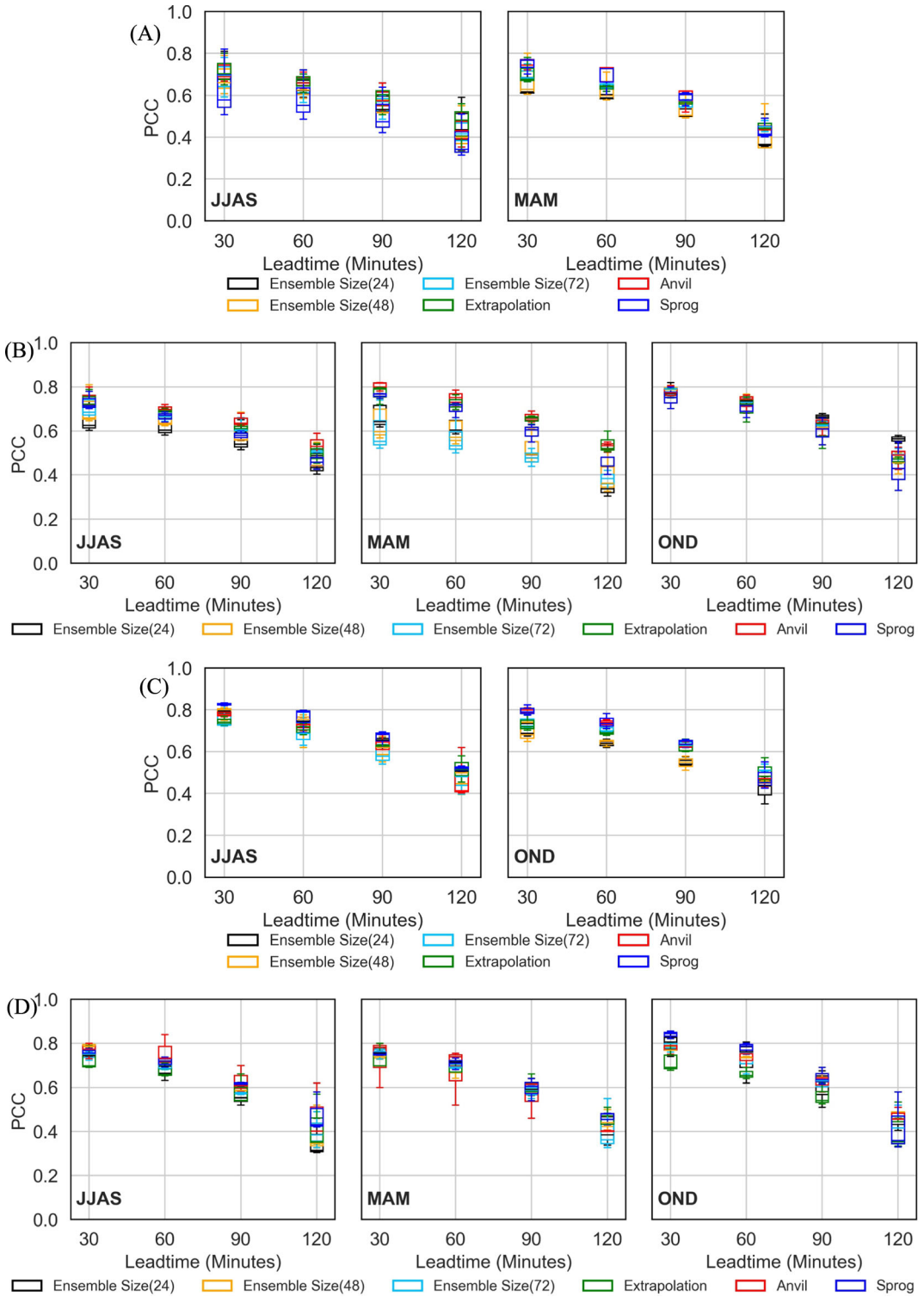

Figure 13. Seasonal performance of PCC (**A**) heavy and (**B**) moderate rain for Agartala; (**C**) heavy and (**D**) moderate rain for Mohanbari.

6.2 *Comparison of CSI*

Kernel density estimation of CSI for all seasons is shown in figure 10(A) for heavy rain with all the algorithms discussed so far. The same for medium rain is presented in figure 10(B) for Agartala. Figure 10(C and D) shows kernel density estimation of CSI for heavy and moderate rain of Mohanbari, respectively, using all the algorithms. For both locations, improved CSI was observed for pre-/post-monsoonal rain compared to monsoonal rain. ANVIL shows better performance for most of

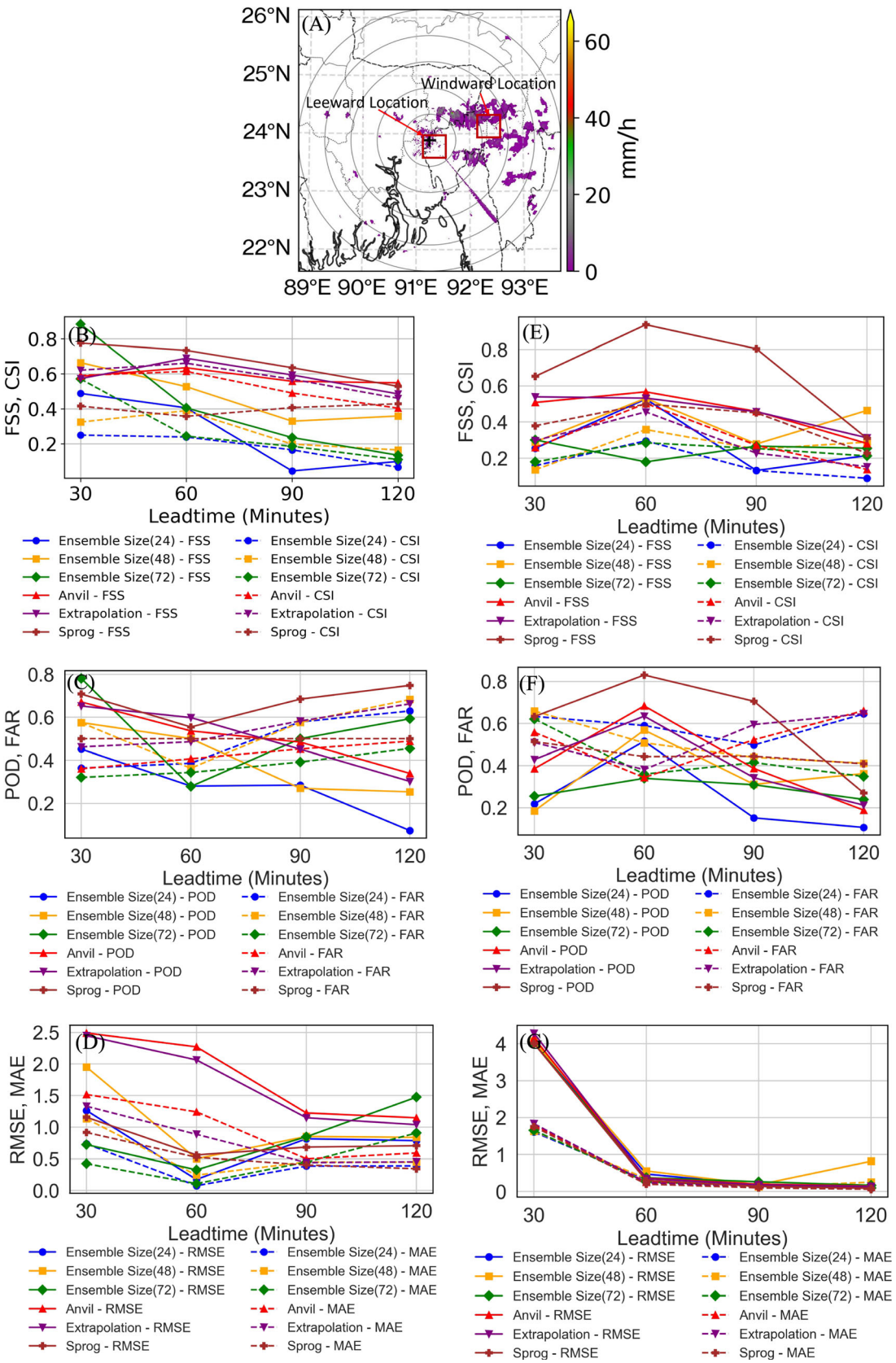

Figure 14. (**A**) Windward and Leeward study location. (**B**) FSS, CSI, (**C**) POD, FAR and (**D**) RMSE, MAE for windward location and (**E**) FSS, CSI, (**F**) POD, FAR and (**G**) RMSE, MAE for leeward location.

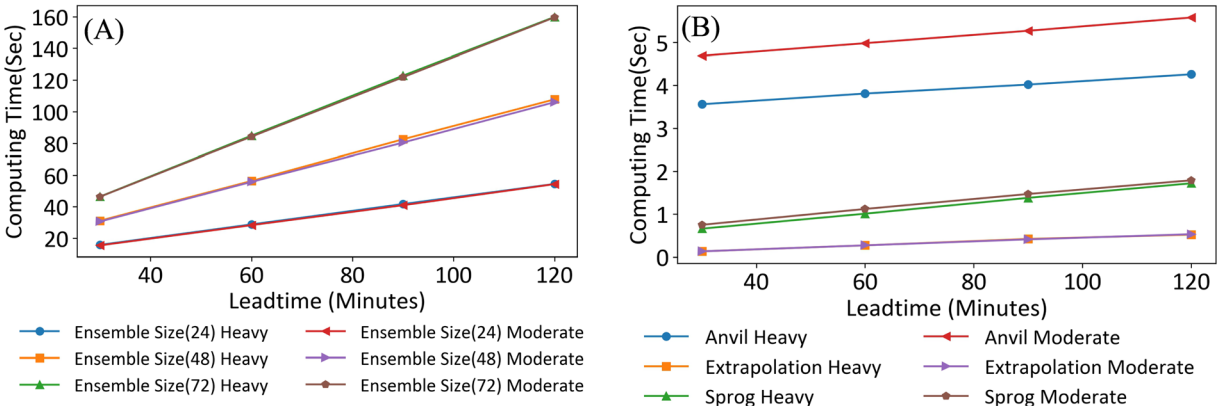

Figure 15. Computing time for (**A**) ensemble-based nowcasting and (**B**) non-ensemble-based nowcasting.

Table 3. *Performance metrics of STEPS algorithm with ensemble size 24, using motion field DARTS and LK.*

Rain category	Performance parameter	Motion field used	Maximum score (lead time 30 min)	Performance parameter	Motion field used	Maximum score (lead time 120 min)
Heavy	FSS	DARTS	0.72	FSS	DARTS	0.64
		LK	0.73		LK	0.62
	CSI	DARTS	0.56	CSI	DARTS	0.47
		LK	0.57		LK	0.48
	POD	DARTS	0.70	POD	DARTS	0.61
		LK	0.71		LK	0.63
	Computing time (sec)	DARTS	15.85	Computing time (sec)	DARTS	54.45
		LK	15.78		LK	54.14
Moderate	FSS	DARTS	0.68	FSS	DARTS	0.61
		LK	0.69		LK	0.54
	CSI	DARTS	0.58	CSI	DARTS	0.52
		LK	0.60		LK	0.46
	POD	DARTS	0.66	POD	DARTS	0.61
		LK	0.68		LK	0.54
	Computing time (sec)	DARTS	15.53	Computing time (sec)	DARTS	54.33
		LK	15.72		LK	54.23

the considered cases, however, in some cases, as indicated in the figure, SPROG shows better performance. Therefore, seasonal and locational dependence are the major considerations while searching for an appropriate algorithm for nowcasting.

6.3 *Comparison of POD and FAR*

The study here focuses on operational hydrological purpose, specifically for exploring an efficient nowcasting method applicable to NE hill India. Therefore, a comparison has been done separately with respect to POD and FAR with increasing lead time. Figure 11(A and B) shows POD and FAR for heavy and moderate rain over Agartala for 5th July 2023 and 28th June 2023, respectively and figure 11(C and D) shows POD and FAR for heavy and moderate rain over Mohanbari for 8th July 2023 and 22nd June 2023, respectively. POD and FAR show improved scores for pre- and post-monsoon months as compared to monsoon months; however, locational and seasonal dependence matter a lot to comment on performance. Interestingly, for some cases of monsoon months, the extrapolation method of nowcast shows even improvised performance. This may be due to some instances in the nowcasting process, where rain cell aggregation and dissociation follow the immediate previous trend.

6.4 *Comparison of statistical performance*

Figure 12(A and B) shows RMSE and MAE for heavy and moderate rain for Agartala, respectively, and figure 12(C and D) shows RMSE and MAE for heavy and moderate rain for Mohanbari, respectively. In the same way, figure 13(A and B) shows PCC for heavy and moderate rain for Agartala, respectively and figure 13(C and D) shows PCC for heavy and moderate rain for Mohanbari, respectively. MAE is consistent across the seasons for all categories of rain for Mohanbari, however, for Agartala, performance with respect to MAE at pre-monsoon and post-monsoon is good as compared to that of monsoon, irrespective of the category of rain. However, performance degradation is not so significant with the increase in lead time. It is observed that for the case of Agartala, the RMSE of non-monsoon period shows better performance as compared to the monsoon period. For Mohanbari, the performance is consistent. PCC for all the cases is observed to be acceptable for up to one and a half hours lead time.

6.5 *Comparison of performance between windward and leeward location*

The presence of hills towards the direction of the rainy motion field significantly affects nowcasting performance. To understand the effect, nowcasting of rain has been studied separately over a windward region, the eastern side of Jampui Hills, Tripura and the leeward region, Agartala, Tripura. The performance score is plotted in figure 14. There is a gradual degradation of performance with an increase in the lead time of FSS and CSI. POD and FAR statistics from the figure also indicate that the choice of algorithm for nowcasting should be location-dependent. Among the statistical parameters, RMSE and MAE decrease with lead time for both locations.

6.6 *Comparison of computing time*

Computing time is a major concern in operational hydrology, especially for nowcasting purpose where immediate action is to be taken to safeguard the livelihood of the NE Indian Himalayan foothills. Computing time variation with lead time for heavy rain, using the ensemble-based algorithm is shown in figure 15(A) and using the non-ensemble-based algorithm is shown in figure 15(B). SPROG shows a very less computing time compared to any method of nowcast except extrapolation. It is even ten times faster than the ensemble-based STEPS method. The overall finding is that with an increase in lead time, model complexity increases. Linear increase of computing time with a very high gradient in the case of STEPS as compared to any non-ensemble-based algorithm of nowcasting has been observed from the figure. However, injecting uncertainty to cope with the real-time situation improves the nowcasting process, sacrificing computational cost.

7. Comparison of performance using DARTS and LK as motion estimator

Performance of two typical cases (heavy rain and moderate rain) using STEPS algorithm with 24 ensemble members, along with DARTS, as well as the LK optical motion estimator, is projected in table 3 for Agartala. The selection of a motion estimator is done considering realistic studies, as per the instance availability for the case. It is seen that for heavy rain, there is negligible variation in performance, whereas for moderate rain, there is a slight variation.

Initially, for a half an hour lead time of prediction, there is almost no variation in FSS, CSI and POD using both DARTS and LK as motion estimator, however, as the lead time of prediction increases to two hours, the use of DARTS is found to be better as compared to LK, resulting in similar computing time.

8. Conclusion

Exhaustive understanding of the blending of orography, fluid dynamics and thermodynamic change of climate is really challenging, and it is the prime requirement for nowcasting of rain. A comparative analysis of the performance of nowcasting has been done using various optical motion field estimators and ensemble as well as non-ensemble-based algorithms over the NE Himalayan hilly Indian tropical region, considering all seasonal variations. All the methods are compared also in terms of computing time to get an estimate of operational use. Main challenges associated with the nowcasting are the short lifetime of a convective cell and sudden changes in storm dynamics. More than 532 samples covering various rain types at various dates of the year 2023 of two NE Himalayan hilly tropical populated locations, Agartala and Mohanbari

region, have been used for this analysis for a varying lead time of half an hour to two hours, even for an intense rain of long duration. The study of performance parameters, including computing time, will help to decide the operational model for nowcasting for Agartala and Mohanbari of the NE hilly Indian region with two hours of lead time for a particular season. The rest of the populated regions, such as Sikkim and Shillong, also face a similar type of widespread long-lasting rain with a sudden, rapid, dynamic change in the life of a rain cell. This study will be helpful when NWP struggles to predict rain with a shorter lead time, like two hours. The PySTEPS module also has a limitation that it can extrapolate the location of the field and intensity, but is unable to develop new fields on the basis of climate thermodynamic parameters. Blending NWP with extrapolation and DWR data as input will provide an improved forecast. Therefore, in the future, other climate parameters such as temperature, pressure, and wind field inclusion in rainfall prediction as input will further improve the quality of nowcasting.

Acknowledgements

This work is financially supported by the Ministry of Earth Science, Government of India (MoES/16/06/2021-RDESS/NARM-6 and MoES/16/04/2021-RDESS/NARM-4). An invaluable support from RADAR Lab, Government of India, is thankfully acknowledged for providing the data.

Author statement

Swastika Chakraborty: Conceptualization, data curation, writing; Sumon Kumar Mondal: Data analysis; Saurabh Das: Supervision, review and editing; and Bipasha Paul Shukla: Review.

References

Anders A M, Roe G H, Hallet B, Montgomery D R, Finnegan N J and Putkonen J 2006 Spatial patterns of precipitation and topography in the Himalaya; In: *Tectonics, Climate, and Landscape Evolution* (eds) Sean D W, Niels H, Mark T B and Donald M F, *Geol. Soc. Am. Spec. Paper, Washington, USA*, https://doi.org/10.1130/2006.2398(03).

Antonio B and Aitchison L 2023 The Fractions Skill Score doesn't always measure skill; *Izv. Atmos. Ocean. Phys. (preprint)*, https://doi.org/10.48550/arXiv.2311.11985.

Banerjee A, Dimri A P and Kumar K 2020 Rainfall over the Himalayan foot-hill region: Present and future; *J. Earth Syst. Sci.* **129** 1–16, https://doi.org/10.1007/s12040-019-1295-2.

Bowler N E, Pierce C E and Seed A W 2020 STEPS: A probabilistic precipitation forecasting scheme which merges an extrapolation nowcast with downscaled NWP; *Q. J. R. Meteorol. Soc.* **132(620)** 2127–2155, https://doi.org/10.1256/qj.04.100.

Bringi V N and Chandrasekar V 2001 *Polarimetric Doppler weather radar: Principles and applications*, UK, Press Syndicate of The University of Cambridge, https://doi.org/10.1017/CBO9780511541094.

Chakraborty S, Saha U and Maitra A 2015 Relationship of convective precipitation with atmospheric heat flux – a regression approach over an Indian tropical location; *Atmos. Res.* **161** 116–124, https://doi.org/10.1016/j.atmosres.2015.04.008.

Chen J, Dai A, Zhang Y and Rasmussen K L 2020 Changes in convective available potential energy and convective inhibition under global warming; *J. Clim.* **33(6)** 2025–2050, https://doi.org/10.1175/JCLI-D-19-0461.1.

Doviak R J 2006 *Doppler Radar and Weather Observations*; 2nd edn, Dover Publications, San Diego, USA, Mineola, N.Y.

Germann U and Joss J 2004 Operational Measurement of Precipitation in Mountainous Terrain; In: *Weather Radar* (ed.) Meischner P, Berlin, Heidelberg, Springer, https://doi.org/10.1007/978-3-662-05202-0_2.

Goyal S, Kumar A, Mohapatra M, Rathore L S, Dube S K, Saxena R and Giri R K 2017 Satellite-based technique for nowcasting of thunderstorms over Indian region; *J. Earth Syst. Sci.* **126** 1–13, https://doi.org/10.1007/s12040-017-0859-2.

Gray W R and Seed A W 2006 The characterisation of orographic rainfall; *Meteorol. Appl.* **7(2)** 105–119, https://doi.org/10.1017/S1350482700001559.

Ha J H and Lee H 2024 A Deep learning model for precipitation nowcasting using multiple optical flow algorithms; *Wea. Forecast.* **39(1)** 41–53, https://doi.org/10.1175/WAF-D-23-0104.1.

Hambali R, Legono D and Jayadi R 2020 The application of pyramid Lucas–Kanade optical flow method for tracking rain motion using high-resolution radar images; *Jurnal Teknologi.* **83(1)** 105–115, https://doi.org/10.11113/jurnalteknologi.v83.14494.

Hamilton J D and Susmel R 1994 Autoregressive conditional heteroskedasticity and changes in regime; *J. Econom.* **64(1–2)** 307–333, https://doi.org/10.1016/0304-4076(94)90067-1.

Han L, Zhang J, Chen H, Zhang W and Yao S 2022 Toward the predictability of a radar-based nowcasting system for different precipitation systems; *IEEE Geosci. Remote Sens. Lett.* **19** 1–5, https://doi.org/10.1109/LGRS.2022.3185031.

Helmus J J and Collis S M 2016 The Python ARM Radar Toolkit (Py-ART), a library for working with weather radar data in the Python programming language; *J. Open Res. Softw.* **4(1)** e25, https://doi.org/10.5334/jors.119.

Imhoff R O, Brauer C C, Overeem A, Weerts A H and Uijlenhoet R 2020 Spatial and temporal evaluation of radar rainfall nowcasting techniques on 1,533 events; *Water Resour. Res.* **56** e2019WR026723, https://doi.org/10.1029/2019WR026723.

Liguori S, Rico-Ramirez M A, Schellart A N A and Saul A J 2012 Using probabilistic radar rainfall nowcasts and NWP forecasts for flow prediction in urban catchments; *Atmos. Res.* **103** 80–95, https://doi.org/10.1016/j.atmosres.2011.05.004.

Paul A R and Maity R 2023 Future projection of climate extremes across contiguous northeast India and Bangladesh; *Sci. Rep.* **13(1)** 15616, https://doi.org/10.1038/s41598-023-42360-2.

Pulkkinen S, Chandrasekar V and Harri A M 2019a Fully spectral method for radar-based precipitation nowcasting; *IEEE J-STARS* **12(5)** 1369–1382, https://doi.org/10.1109/JSTARS.2019.2908974.

Pulkkinen S, Nerini D, Pérez Hortal A A, Velasco-Forero C, Seed A, Germann U and Foresti L 2019b PySTEPS: An open-source Python library for probabilistic precipitation nowcasting (v1. 0); *Geosci. Model Dev.* **12(10)** 4185–4219, https://doi.org/10.5194/gmd-12-4185-2019.

Pulkkinen S, Chandrasekar V, von Lerber A and Harri A M 2020 Nowcasting of convective rainfall using volumetric radar observations; *IEEE TGRS* **58(11)** 7845–7859, https://doi.org/10.1109/TGRS.2020.2984594.

Raj B, Sahoo S, Puviarasan N and Chandrasekar V 2024 Operational assessment of high resolution weather radar based precipitation nowcasting system; *Atmosphere* **15(2)** 154, https://doi.org/10.3390/atmos15020154.

Ray K, Bandopadhyay B K and Bhan S C 2015 Operational nowcasting of thunderstorms in India and its verification; *Mausam* **66(3)** 595–602, https://doi.org/10.54302/mausam.v66i3.566.

Reinoso-Rondinel R, Rempel M, Schultze M and Trömel S 2022 Nationwide radar-based precipitation nowcasting – A localization filtering approach and its application for Germany; *IEEE J-STARS* **15** 1670–1691, https://doi.org/10.1109/JSTARS.2022.3144342.

Robert A 1982 Cloud clusters and large-scale vertical motions in the tropics; *J. Meteorol. Soc. Jpn.* **60(1)**, https://doi.org/10.2151/jmsj1965.60.1_396.

Roberts N M and Lean H W 2008 Scale-selective verification of rainfall accumulations from high-resolution forecasts of convective events; *Mon. Weather Rev.* **136(1)** 78–97, https://doi.org/10.1175/2007MWR2123.1.

Ruzanski E, Wang Y and Chandrasekar V 2009 Development of a real-time dynamic and adaptive nowcasting system; In: *Proceedings of the 25th International Conference on Interactive Information and Processing Systems for Meteorology, Oceanography, and Hydrology*, Arizona, USA, 11–15 January 2009.

Saha P, Mahanta R and Goswami B N 2023 Present and future of the South Asian summer monsoon's rainy season over Northeast India; *npj Clim. Atmos. Sci.* **6(1)** 170, https://doi.org/10.1038/s41612-023-00485-1.

Schmid W, Schiesser H H and Waldvogel A 1992 The kinetic energy of hailfalls. Part IV: Patterns of hailpad and radar data; *J. Appl. Meteorol.* **31** 1165–1178, https://doi.org/10.1175/1520-0450(1992)031%3c1165:TKEOHP%3e2.0.CO;2.

Sen Roy S, Saha S B, Roy Bhowmik S K and Kundu P K 2014 Optimization of Nowcast Software WDSS-II for operational application over the Indian region; *Meteorol. Atmos. Phys.* **124** 143–166, https://doi.org/10.1007/s00703-014-0315-7.

Shrestha D, Singh P and Nakamura K 2012 Spatiotemporal variation of rainfall over the central Himalayan region revealed by TRMM Precipitation Radar; *J. Geophys. Res. Atmos.* **117(D22)**, https://doi.org/10.1029/2012JD018140.

Singh N, Shukla B P, Kaushik N, Varma A K, Mitra A K and Bhan S C 2023 Validation of INSAT-3D/3DR based nowcasting rain occurrences for heavy rainfall using hydro-estimator product; *Adv. Space Res.* **72(6)** 2185–2194, https://doi.org/10.1016/j.asr.2023.05.030.

Singh P and Kumar N 1997 Effect of orography on precipitation in the western Himalayan region; *J. Hydrol.* **199(1–2)** 183–206, https://doi.org/10.1016/S0022-1694(96)03222-2.

Skolnik M I 1980 *Introduction to Radar Systems* (ed.) Frank J C, 2nd edn, New York, McGraw Hill Book Company Inc., 500p.

Smith R B 1979 The influence of mountains on the atmosphere; *Adv. Geophys.* **21** 87–230, https://doi.org/10.1016/S0065-2687(08)60262-9.

Srivastava A, Kumar P, Panda S K, Das A K, Pattanaik D R and Mohapatra M 2024 Development of India Meteorological Department: High Resolution Rapid Refresh (IMD-HRRR) modeling system for very short range weather forecasting; *Pure Appl. Geophys.* **181(11)** 3393–3408, https://doi.org/10.1007/s00024-024-03549-2.

Srivastava K, Lau S Y, Yeung H Y, Cheng T L, Bhardwaj R, Kannan A M, Bhowmik S R and Singh H 2012 Use of SWIRLS nowcasting system for quantitative precipitation forecast using Indian DWR data; *Mausam* **63(1)** 1–16, https://doi.org/10.54302/mausam.v63i1.1442.

Wilson J W, Crook N A, Mueller C K, Sun J and Dixon M 1998 Nowcasting thunderstorms: A status report; *Bull. Am. Meteorol. Soc.* **79(10)** 2079–2100, https://doi.org/10.1175/1520-0477(1998).

Wilson J W, Ebert E E, Saxen T R, Roberts R D, Mueller C K, Sleigh M, Pierce C E and Seed A 2004 Sydney 2000 forecast demonstration project: Convective storm nowcasting; *Wea. Forecast.* **19(1)** 131–150, https://doi.org/10.1175/1520-0434(2004)019%3c0131:SFDPCS%3e2.0.CO;2.

Zahan Y, Mahanta R, Rajesh P V and Goswami B N 2021 Impact of climate change on North-East India (NEI) summer monsoon rainfall; *Clim. Change.* **164** 1–19, https://doi.org/10.1007/s10584-021-02994-5.

Zhu J and Dai J 2022 A rain-type adaptive optical flow method and its application in tropical cyclone rainfall nowcasting; *Front. Earth Sci.* **16** 248–264, https://doi.org/10.1007/s11707-021-0883-z.

Corresponding editor: Parthasarathi Mukhopadhyay